Available on the CERN CDS information server **CMS PAS B2G-17-002**

CMS Physics Analysis Summary

Contact: cms-pag-conveners-b2g@cern.ch 2017/03/23

Search for heavy resonances decaying into a vector boson and a Higgs boson in hadronic final states with 2016 data

The CMS Collaboration

Abstract

A search for heavy resonances with a mass above 1 TeV, decaying to a vector boson and a Higgs boson is presented. The search considers hadronic decays of the vector boson, and Higgs boson decays to b quarks. The collimated pair of quarks are reconstructed as a single massive jet. The analysis is performed using a data sample collected in 2016 by the CMS experiment at the LHC in proton-proton collisions at a center-of-mass energy of 13 TeV, corresponding to an integrated luminosity of 35.9 fb^{-1}. The data is found to be consistent with the background expectation and used to place limits in the context of a theoretical model with a heavy vector triplet. In the benchmark scenario model B, a resonance with mass up to 3.4 TeV is excluded at 95% confidence level, and stringent limits are set on the parameters of the model.

1 Introduction

The discovery of the Higgs boson H at the CERN LHC [1–3] sets a milestone in the understanding of the standard model (SM) of particle physics. However, the amount of fine-tuning required to accommodate a mass of 125 GeV [4–7] suggests the presence of new heavy particles beyond the SM (BSM) above the TeV scale, which can be within the reach of the LHC. These resonances are expected to be connected to the electroweak sector of the SM, with significant couplings to the SM gauge boson. Hence, the decay of heavy resonances into a vector boson (W or Z) and a Higgs boson represents a possible signature for their observation.

These processes are predicted by several BSM theories, most notably weakly coupled spin-1 Z′ [8, 9] and W′ models [10], strongly coupled Composite Higgs [11–13], and Little Higgs models [14–16]. These models are generalized in the heavy vector triplet (HVT) framework [17], which extends the SM by introducing a triplet of heavy vector bosons, one neutral Z′ and two charged W′, collectively represented as V′. The heavy vectors couple to SM bosons and fermions with strength $g_{\mathrm{V}}c_{\mathrm{H}}$ and $g^2c_{\mathrm{F}}/g_{\mathrm{V}}$, where g_{V} is the strength of the new interaction, c_{H} the coupling between the heavy vector bosons, the Higgs boson, and longitudinally polarized SM vector bosons, c_{F} the coupling between the HVT bosons and the SM fermions, and g the electroweak coupling constant. In this search, two different benchmark scenarios are considered [17]. In the model A ($g_{\mathrm{V}} = 1$) scenario, the coupling strength with the SM bosons and fermions is comparable, and the new particles decay primarily to fermions. In the model B ($g_{\mathrm{V}} = 3$) scenario the couplings to fermions are suppressed with respect to the couplings to bosons, resulting in a branching fraction to SM bosons close to unity.

This note describes the search for heavy resonances decaying into a SM vector boson and a Higgs boson, which subsequently decay into a pair of quarks and a pair of b quarks, respectively. In spite of the overwhelming multijet background, the hadronic decay modes take advantage of the large branching fractions. With resonance masses above the TeV scale [18–27], the two bosons produced in the decay would have large Lorentz boosts in the laboratory frame, and consequently the quarks generated by each boson tend to be clustered within a single hadronic jet. The analysis of the jet mass, substructure, and b tagging information provides crucial information to identify genuine hadronically-decaying vector bosons or Higgs boson candidates, and discriminate against the dominant SM backgrounds.

This search complements and significantly extends the reach of the CMS search for VH resonances with semileptonic decay modes of the vector bosons [28], which excludes at 95% confidence level (CL) W′ and Z′ resonances with mass below 1.6 TeV and a combined V′ resonance with mass up to 2.0 TeV in the HVT benchmark model B. ATLAS also performed a search in the same final state, excluding W′ and Z′ below 2.2 and 1.6 TeV, respectively, considering the same scenario [29]. In the hadronic channel and with a larger data set, ATLAS excluded W′ and Z′ resonances with mass smaller than 2.5 and 1.6 TeV in the HVT model B, observing an excess with a local significance of 3.5 standard deviations at $m_{\mathrm{W}'} \sim 3.0$ TeV [30].

2 Data and simulated samples

The data sample analyzed in this analysis was collected with the CMS detector in proton-proton collisions at a center-of-mass energy of 13 TeV during 2016, and corresponds to an integrated luminosity of 35.9 fb^{-1}.

Simulated signal events are generated at leading order (LO) with the MADGRAPH5_aMC@NLO v5.2.2.2 matrix element generator [31]. The Higgs boson is required to decay into a $\mathrm{b\bar{b}}$ pair,

and the vector boson decays into a pair of quarks. Different m_X hypotheses in the range 1000 to 4500 GeV are considered, assuming a narrow resonance width (0.1% of the mass), which is smaller with respect to the experimental resolution. This approximation is valid in a large fraction of the HVT parameter space, and fulfilled in benchmark model A ($g_V = 1$) and model B ($g_V = 3$) [17]. Multijet background events are generated at LO with MADGRAPH5_aMC@NLO, and top quark pair production is simulated at next-to-leading order (NLO) POWHEG v2 generator [32–34] and rescaled to the cross section computed with TOP++ v2.0 [35] at next-to-next-to-leading order. Other SM backgrounds, such as W+jets, Z+jets, single top production, VV and VH production, are simulated at NLO with MADGRAPH5_aMC@NLO. Parton showering and hadronization processes are simulated by interfacing the event generators to PYTHIA 8.205 [36, 37] with the CUETP8M1 [38, 39] tune. The CUETP8M2T4 tune [40] is used for top quark pair production. The NNPDF 3.0 [41] parton distribution functions (PDFs) are used to model the momentum distribution of the colliding partons inside the protons. Generated events, including additional proton-proton interactions within the same bunch crossing (pileup) corresponding to the average number of interactions per bunch crossing that was observed in 2016 data taking, are processed through a full detector simulation based on GEANT4 [42] and reconstructed with the same algorithms used for data.

3 CMS detector

The central feature of the CMS detector is a superconducting solenoid with a 6 m internal diameter. Within the solenoid volume, a silicon pixel and strip tracker measures charged particles within the pseudorapidity range $|\eta| < 2.5$. It consists of 1440 silicon pixel and 15 148 silicon strip detector modules and is located in the 3.8 T field of the solenoid. For non-isolated particles of transverse momentum $1 < p_T < 10$ GeV and $|\eta| < 1.4$, the track resolutions are typically 1.5% in p_T and 25–90 (45–150) μm in the transverse (longitudinal) impact parameter [43]. A lead tungstate crystal electromagnetic calorimeter (ECAL), and a brass and scintillator hadron calorimeter (HCAL), each composed of a barrel and two endcap sections, provide coverage up to $|\eta| < 3.0$, which is further extended by forward calorimeters [44]. Muons are measured in drift tubes, cathode strip chambers, and resistive-plate chambers embedded in the steel flux-return yoke outside the solenoid.

The first level (L1) of the CMS trigger system [45], composed of custom hardware processors, uses information from the calorimeters and muon detectors to select the most interesting events in a fixed time interval of less than 4 μs. The high-level trigger (HLT) processor farm decreases the event rate from around 100 kHz to about 1 kHz, before data storage.

A detailed description of the CMS detector, together with a definition of the coordinate system used and the relevant kinematic variables, can be found in Ref. [44].

4 Event reconstruction

The event reconstruction is performed using the particle-flow (PF) algorithm [46, 47], which uses an optimized combination of information from the various elements of the CMS detector to reconstruct and identify individual particles produced in each collision. The algorithm identifies each reconstructed particle either as an electron, a muon, a photon, a charged hadron, or a neutral hadron. The PF candidates are clustered into jets using the anti-k_T algorithm [48] with a distance parameter $R = 0.8$, after passing the charged hadron subtraction (CHS) pileup mitigation algorithm. The CHS algorithm [49] discards charged particles depending on the longitudinal impact parameter of the track and considered not to originate from the primary

vertex of the event, identified as the one with the highest sum of the p_T^2 of the associated clustered particles. The residual contamination removed is proportional to the event energy density and the jet area estimated using the FASTJET package [50, 51]. Jet energy corrections, extracted from simulation and data in multijet, γ+jets, and Z+jets events, are applied as a function of the transverse momentum and pseudorapidity to correct the jet response and to account for residual differences between data and simulation. The jet energy resolution typically amounts to 5% at 1 TeV [52]. Jets are required to pass identification criteria, which has negligible impact on the signal efficiency, in order to remove spurious jets arising from detector noise.

A more sophisticated algorithm, denoted as pileup per particle identification (PUPPI) [53], is used to determine exclusively the mass of the jet and the substructure variables. PUPPI uses a combination of local shape information, event pileup properties and tracking information in order to compute a weight describing the likelihood for each particle to originate from pileup interactions. The weight is used to rescale the particle four-momenta, superseding the need for further jet-based corrections. The PUPPI constituents are subsequently clustered with the same algorithm used for CHS jets, and then matched to the AK8 jets clustered with the CHS constituents.

The soft drop algorithm [54, 55], which is designed to remove contributions from soft radiation and additional interactions, is applied to AK8 PUPPI jets. The soft drop jet mass is defined as the invariant mass associated with the four-momentum of the soft drop jet. Dedicated mass corrections, derived from data in a region enriched with $\mathrm{t\bar{t}}$ events with merged $\mathrm{W(q\bar{q})}$ decays, are applied to the jet mass in order to remove residual jet p_T dependence [56]. The measured soft drop PUPPI jet mass resolution is approximately 10%.

Substructure variables are used to identify jets originating from more than one parton. The constituents of the jet are clustered again with the k_T algorithm, and the procedure is stopped when N subjets are obtained. A variable, the N-subjettiness [57], calculated on the jet before the grooming procedure including the PUPPI algorithm corrections for pileup mitigation, is introduced:

$$\tau_N = \frac{1}{d_0} \sum_k p_{T,k} min(\Delta R_{1,k}, \Delta R_{2,k}, \ldots, \Delta R_{N,k})$$

where the index k runs over the jet constituents and the distances $\Delta R_{N,k}$ are calculated with respect to the axis of the N-th subjet, obtained by one iteration of τ minimization by varying the subjet axes around the k_T subjet axes. The normalization factor d_0 is calculated as $d_0 = \sum_k p_{T,k} R_0$, setting R_0 to the radius of the original jet. The variable that best discriminates between light or gluon jets and jets originated by the two body decay of massive particles is the ratio of 2-subjettiness and 1-subjettiness, $\tau_{21} = \tau_2/\tau_1$, which lies in the interval from 0 to 1, where small values correspond to a high compatibility with the hypothesis of a massive object decaying into two quarks. The correction factors relative to the τ_{21} selection are measured from data in a sample enriched in $\mathrm{t\bar{t}}$ events in two τ_{21} intervals (0.99 ± 0.11 for $\tau_{21} < 0.35$, and 1.03 ± 0.23 for $0.35 < \tau_{21} < 0.75$) [56]. These two selections are approximately 50% and 45% efficient on two-pronged jets originated by the decay of a massive boson, and 10% and 60% efficient on one-pronged jets, respectively. The threshold values are chosen in order to maximize the overall sensitivity over the entire mass spectrum.

Higgs boson jet candidates are identified using a dedicated b tagging discriminator, specifically designed to identify a pair of b quarks clustered in a single jet [58]. The algorithm combines information from displaced tracks, secondary vertices and two-secondary vertices system within the Higgs boson jet in a dedicated multivariate algorithm. The decay chains of the two b hadrons are resolved by associating reconstructed secondary vertices to the two N-subjettiness

axes directions. A tight and a loose operating points are chosen to be approximately 35 and 75% efficient, respectively, for Higgs boson jets, with a false-positive rate for light-flavor jets of about 0.8 and 8%. Scale factors, derived from data in muon-enriched events, are applied to the simulation to correct for the different efficiency in data and simulation.

5 Event selection

Events are collected with three set of triggers. The first set requires H_T, defined as the scalar sum of the p_T of the jets, to be larger than 800 or 900 GeV, depending on the instantaneous luminosity. A subset of triggers, with a lower H_T threshold set to 650 GeV, are required also to have a pair of jets whose invariant mass is larger than 950 GeV, and their $\Delta\eta$ to be smaller than 1.5. A second set requires at least one jet with p_T larger than 450 GeV to be reconstructed at the HLT. A third set selects events with at least one jet with $p_T > 360$ GeV passing a trimmed mass [59] requirement of 30 GeV, or $H_T > 700$ GeV and trimmed mass larger than 50 GeV.

In the offline preselection, the two highest-p_T jets in the event are required to have $p_T > 200$ GeV and $|\eta| < 2.5$, and their pseudorapidity separation $|\Delta\eta|$ has to be smaller than 1.3. At least one of the two jets has to have a soft drop jet mass compatible with the Higgs boson mass, $105 < m_j < 135$ GeV (H-jet), and the other a jet mass compatible with the mass of the vector bosons, $65 < m_j < 105$ GeV (V-jet). The jet mass categorization is shown in Fig. 1. The H-jet and V-jet candidates are required to have an invariant mass m_{VH} to be larger than 985 GeV, in order to ensure the full trigger efficiency and avoid turn-on effects. Events with isolated leptons (e, μ) with $p_T > 10$ GeV, or τ-leptons with $p_T > 20$ GeV are rejected. The reconstructed missing energy, calculated as the negative vectorial sum of the transverse momenta of the reconstructed particles and jets in the detector, is required to be smaller than 250 GeV, otherwise the event is discarded.

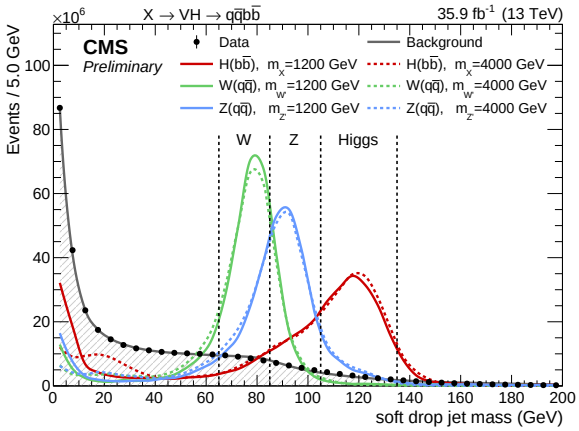

Figure 1: Distribution of the soft drop PUPPI mass for data, simulated background and signal. The distributions are normalized to the number of events observed in data. The dashed vertical lines represent the boundary values of the jet mass categories.

The events passing the preselection are divided into 8 exclusive categories. In order to discriminate against the copious light quark production, two categories are defined for the H-jet, depending on its b tagging discriminator: the *tight* category accepts events with a value larger than 0.9, while the *loose* category selects events with a value between 0.3 and 0.9. V-jets are selected by requiring $\tau_{21} \leq 0.35$ to enter the *high purity* category (HP), and $0.35 < \tau_{21} < 0.75$ for the *low purity* (LP) category. Although it is expected that the tight and high purity categories dominate the total sensitivity, the loose and low purity categories are retained given

the non-negligible signal efficiency with only moderate background contamination for large dijet invariant mass. Two further categories are defined according to the V-jet mass by splitting further the mass interval. Events with V-jet mass closer to the nominal W mass value, $65 < m_j \leq 85\,\text{GeV}$, belong to the *W mass* category, and those with $85 < m_j \leq 105\,\text{GeV}$ fall into the *Z mass* category. Even if the W and Z mass peaks cannot be fully resolved, this classification allows a partial discrimination between a potential W′ or Z′ signal. The signal efficiency for the combination of the eight categories reaches 36% at $m_X = 1.2 - 1.6\,\text{TeV}$, and slowly decreases to 21% at $m_X = 4.5\,\text{TeV}$. The N-subjettiness and b tagging categorizations are shown in Fig. 2.

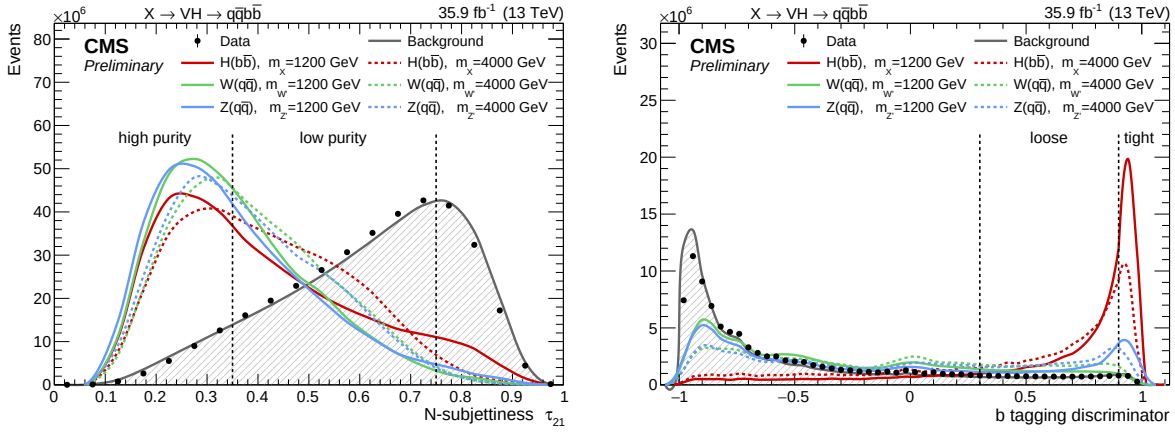

Figure 2: Distribution of the N-subjettiness τ_{21} (left) and b tagging discriminator output (right) for data, simulated background and the signal. The distributions are normalized to the number of events observed in data. The dashed vertical lines represent the boundary values of the categories as described in the text.

6 Estimated and observed background

The background is largely dominated by multijet production, which accounts for more than 95% of the total. The top quark pair contribution is approximately 3–4%, depending on the category. The remaining fraction is composed of vector boson production in association with partons, and SM diboson processes.

The background is estimated directly from data, assuming that it can be described by a smooth, parametrizable, monotonically decreasing function. This assumption is verified in the V-jet mass sidebands ($40 < m_j < 65\,\text{GeV}$) and in simulation. The functions considered are power laws of the variable $x = m_{VH}/\sqrt{s}$, where $\sqrt{s} = 13\,\text{TeV}$ is the center of mass energy, and the number of parameters p, including the normalization, is comprised between 2 and 5:

2 parameters: $p_0 \cdot \frac{1}{(x)^{p_1}}$

3 parameters: $p_0 \cdot \frac{(1-x)^{p_1}}{(x)^{p_2}}$

4 parameters: $p_0 \cdot \frac{(1-x)^{p_1}}{(x)^{p_2+p_3 \cdot \log(x)}}$

5 parameters: $p_0 \cdot \frac{(1-x)^{p_1}}{(x)^{p_2+p_3 \cdot \log(x)+p_4 \cdot \log^2(x)}}$

Starting from the simplest functional form, an iterative procedure based on the Fisher F-test is used to check at 10% CL if additional parameters are needed to model the individual background distributions. For most of the categories, the two-parameter functional form is found

to describe the data spectrum sufficiently well. However, in more populated categories, with loose b tagging or low purity, three- or four-parameter functions are preferred.

The results of the fits are shown in Figs. 3 and 4 for the W and Z mass regions, respectively. The fit range is chosen such that it starts where the trigger efficiency has reached its plateau to avoid any bias from trigger inefficiency. The binning chosen to present the results is related to the detector resolution. The event with the highest invariant mass $m_{\mathrm{VH}} = 4919\,\mathrm{GeV}$ is observed in the W mass, low purity, tight b tag category.

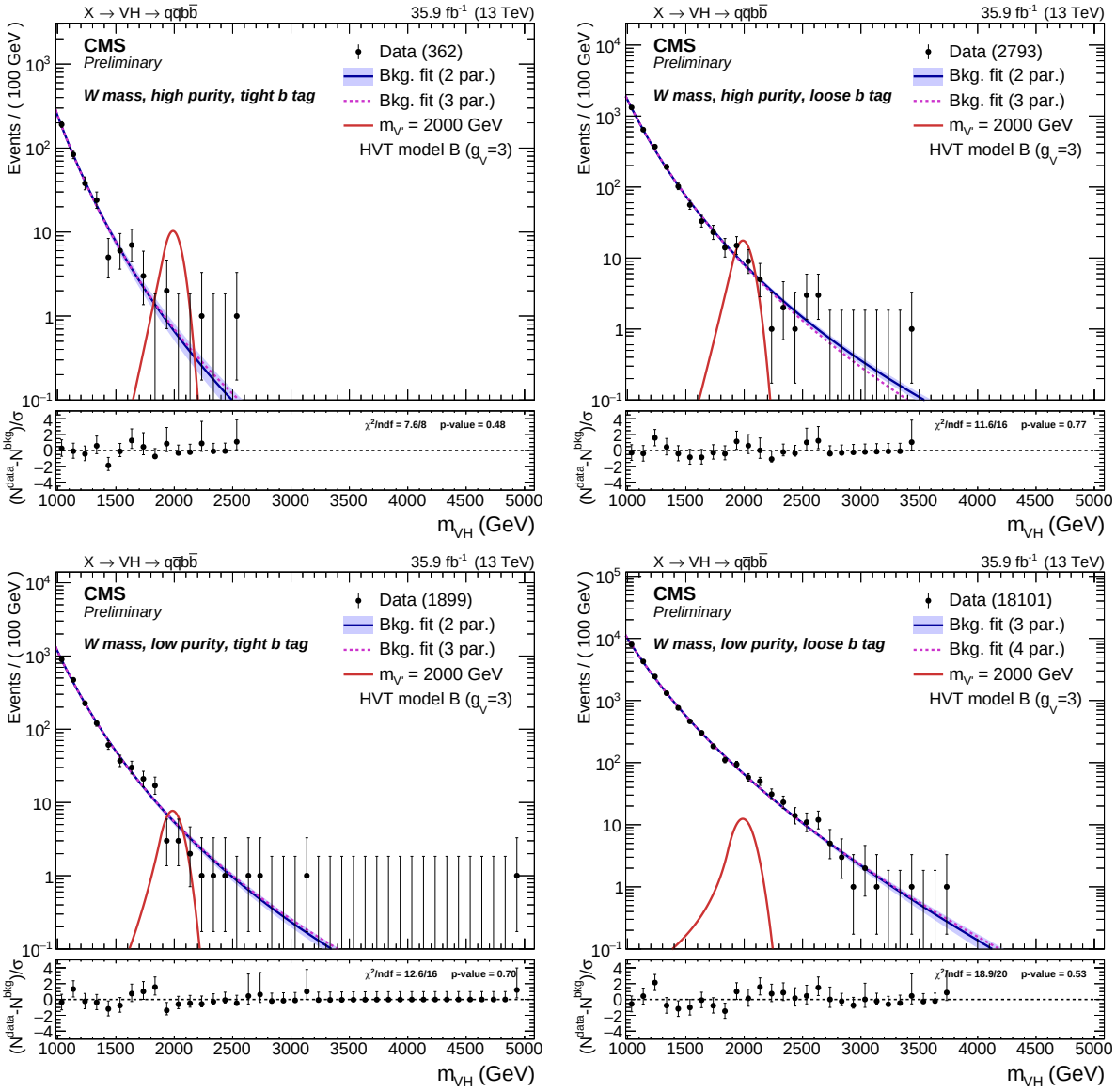

Figure 3: Dijet invariant distribution m_{VH} of the two leading jets in the W mass region: high purity (top) and low purity (bottom) categories, with tight (left) and loose (right) b tagging selections. The observed data are indicated by black markers, and the potential contribution of a resonance with $m_{\mathrm{X}} = 2000\,\mathrm{GeV}$ produced in the context of the HVT model B with $g_{\mathrm{V}} = 3$ is shown with a solid red line. The main and alternative functions shown represent the background-only fit. The bottom panels report the pulls in each bin, $(N^{\mathrm{data}} - N^{\mathrm{bkg}})/\sigma$, where σ is the Poisson uncertainty in data. The error bars represent the normalized Poisson errors on the data and are shown also for bins with zero entries up to the highest m_{VH} event.

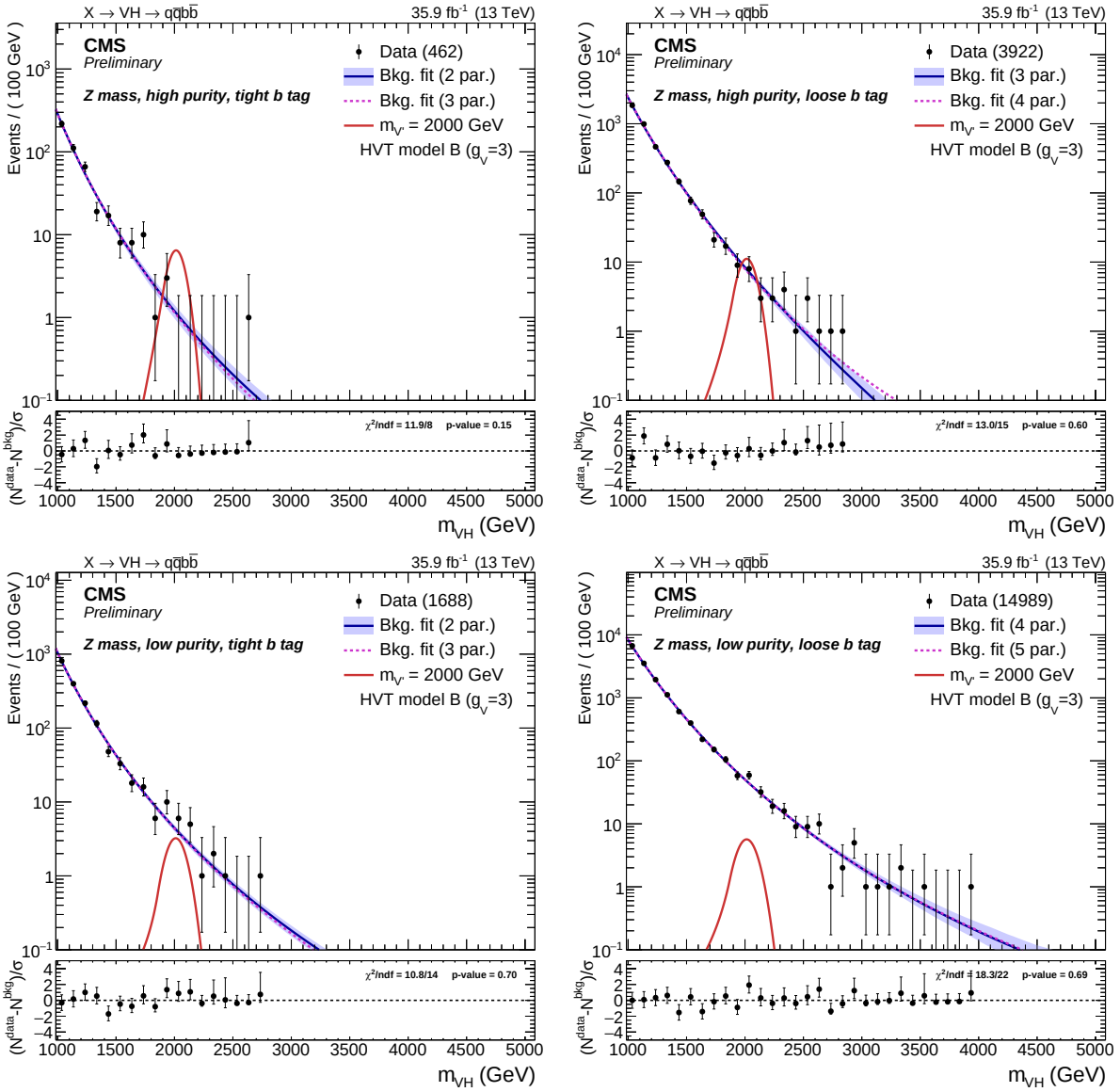

Figure 4: Dijet invariant distribution m_{VH} of the two leading jets in the Z mass region: high purity (top) and low purity (bottom) categories, with tight (left) and loose (right) b tagging selections. The observed data are indicated by black markers, and the potential contribution of a resonance with $m_{\mathrm{X}} = 2000\,\mathrm{GeV}$ produced in the context of the HVT model B with $g_{\mathrm{V}} = 3$ is shown with a solid red line. The main and alternative functions shown represent the background-only fit. The bottom panels report the pulls in each bin, $(N^{\mathrm{data}} - N^{\mathrm{bkg}})/\sigma$, where σ is the Poisson uncertainty in data. The error bars represent the normalized Poisson errors on the data and are shown also for bins with zero entries up to the highest m_{VH} event.

The shape of the reconstructed signal mass distribution is extracted from the simulated signal samples. The signal shape is parametrized separately for each channel with a Gaussian peak and a power law to model the lower tail, for a total of 4 parameters. The resolution of the reconstructed m_{VH} is given by the width of the Gaussian core, and is found to be 4% at low and 3% at high resonance masses.

Dedicated tests have been performed to check the robustness of the fit method by generating pseudo-experiments after injecting a simulated signal with different mass values and cross sections. The pseudo-data distribution is then fitted with the function chosen by repeating the F-test procedure. The fitted signal yield is found to be compatible within one third of the statistical uncertainty to the injected yield, regardless of the injected signal strength and resonance mass. These tests confirm that the choice of the function used to model the background or the presence of a potential signal in real data would not introduce a significant bias in the background estimation.

7 Systematic uncertainties

The background estimation is obtained from the fit to the data in the considered categories. As such, the only relevant uncertainty originates from the covariance matrix of the dijet function fit. While different parametrizations of the fit function were studied, the observed variations are within the bounds of the aforementioned uncertainty and are assumed to pose no additional source of uncertainty.

The dominant uncertainties on the signal arise from the H-jet and V-jet tagging. The b tagging scale factor uncertainties [58] are varied by one standard deviation, and the difference in the signal yield is estimated to be 4–8% for the tight categories and 2–5% for the loose categories. The same procedure is applied to the τ_{21} scale factors, whose uncertainty is reported in Sec. 4. The uncertainties relative to the Higgs boson mass selection and the V-jet tagging extrapolation at larger jet p_{T} are estimated by using an alternative HERWIG [60] shower model, and are quantified as 5–7% and 3–20% for the H and V jet candidates, respectively.

Uncertainties on the reconstruction of the hadronic jets affect both the signal efficiency and the shape of the reconstructed resonance mass. The four-momenta of the reconstructed jets are scaled and smeared according to the uncertainties on the jet p_{T} and momentum resolution. These effects account for a 1% uncertainty on the mean, and 2% of the width of the signal Gaussian core. The jet mass is also scaled and smeared according to the measurement of the jet mass scale and resolution, inducing a 2% and 10% normalization uncertainty, respectively, and a 4–6% and 5% migration effect between the W and Z mass regions.

Additional systematic uncertainties affecting the signal normalization include the lepton and missing energy vetoes (accounting for 1% each), pileup contributions (0.1%), the integrated luminosity (2.6%) [61], and the choice of the parton distribution functions set [62] (1% for acceptance, 6–25% for the scale). The factorization and renormalization scale uncertainties are estimated by varying the scales up and down by a factor of 2, and the resulting effect is a variation of 4–13% of the normalization of the signal events.

8 Results and interpretation

Results are obtained by separately fitting the background functions and the signal shape to the unbinned data m_{VH} distributions in the corresponding categories across all search regions. In the fit, based on a profile likelihood, the parameters and the normalization of the background in

each category are free to float. Systematic uncertainties are treated as nuisance parameters and are profiled in the statistical interpretation [63–66]. The background-only hypothesis is tested against the $X \to VH$ signal in the 8 exclusive categories. The asymptotic modified frequentist method is used to determine limits at 95% CL on the contribution from signal. Limits are derived on the product of the cross section for a heavy vector boson X and the branching fractions for the decays $X \to VH$ and $H \to b\bar{b}$, denoted $\sigma(X)\,\mathcal{B}(X \to VH)\,\mathcal{B}(H \to b\bar{b})$. No specific assumption is made on $\mathcal{B}(H \to b\bar{b})$, since this decay channel has not yet been measured.

The results are presented in the spin-1 W′ or Z′ heavy singlet hypothesis, and shown in Fig. 5 and compared to the cross sections expected in HVT model A ($g_V = 1$) and model B ($g_V = 3$). The uncertainties on the PDF scale, and factorization and renormalization scale are not profiled in the likelihood fit, as they are reported separately as uncertainties on the model cross section. With the current data set, a narrow W′ resonance with $m_{W'} \leq 3.27$ and 3.10 TeV can be excluded at 95% CL, except in a limited region between 2.54–2.76 TeV and 2.46–2.82 TeV, as well as Z′ resonance with $m_{Z'} \leq 2.41$ and 2.31 TeV in the HVT model B ($g_V = 3$) and model A ($g_V = 1$), respectively. The exclusion limits for the heavy vector triplet hypothesis are also presented in Fig. 6, excluding a mass range from 1.00–2.66 and 2.72–3.39 TeV in the benchmark model B and significantly extending the reach with respect to the $\sqrt{s} = 8$ TeV and $\sqrt{s} = 13$ TeV CMS searches [19, 28]. In model A, the excluded range is between 1.00–2.51 TeV and 2.80–3.26 TeV. The excess observed by ATLAS with a local significance of 3.5 standard deviations at $m_{W'} \sim 3.0$ TeV [30] is not confirmed.

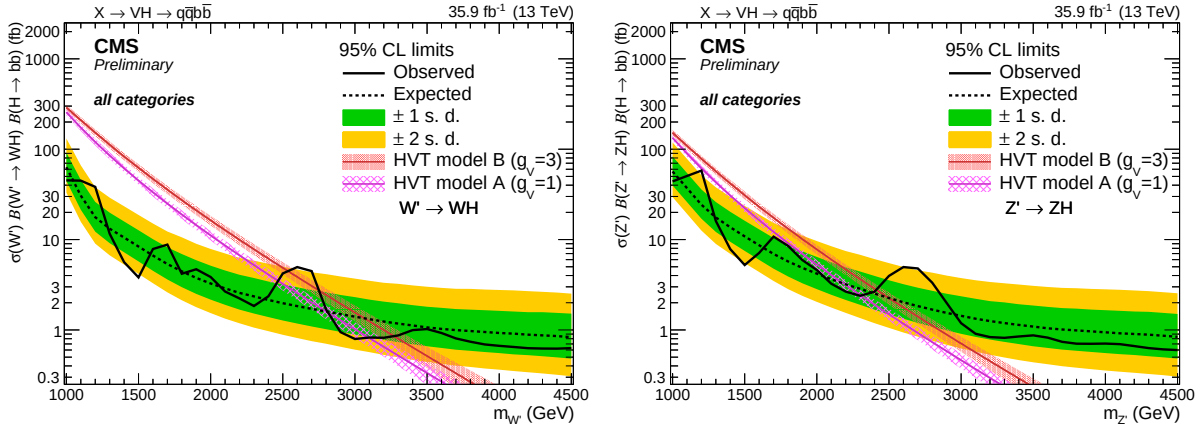

Figure 5: Observed and expected 95% CL upper limits on $\sigma(W')\,\mathcal{B}(W' \to WH)\,\mathcal{B}(H \to b\bar{b})$ (left) and $\sigma(Z')\,\mathcal{B}(Z' \to ZH)\,\mathcal{B}(H \to b\bar{b})$ (right) as a function of the resonance mass for a single narrow spin-1 resonance, including all statistical and systematic uncertainties. The inner green and outer yellow bands represent the ± 1 and ± 2 standard deviation uncertainties on the expected limit. The red and purple solid curves correspond to the cross sections predicted by the HVT model B ($g_V = 3$) and model A ($g_V = 1$), respectively.

The exclusion limit shown in Fig. 6 can be interpreted as a function of the coupling strength of the heavy vectors to the SM bosons and fermions in the $[g_V c_H,\ g^2 c_F / g_V]$ plane. The excluded region of the parameter space for narrow resonances relative to the combination of all the considered channels is shown in Fig. 7. The fraction of the parameter space where the natural width of the resonances is larger than the typical experimental resolution of 4%, and thus the narrow width approximation is not valid, is also indicated in Fig. 7.

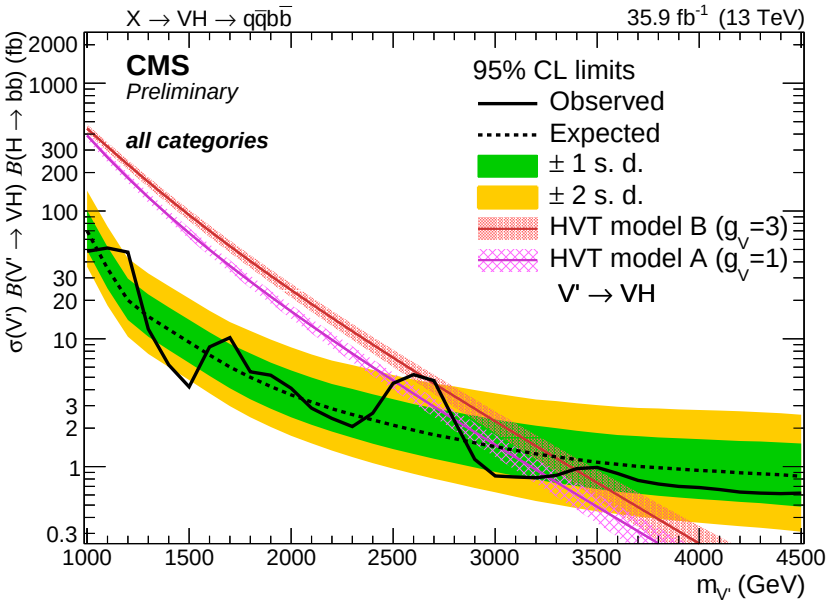

Figure 6: Observed and expected 95% CL upper limit with the ± 1 and ± 2 standard deviation uncertainty bands on $\sigma(\mathrm{X})\,\mathcal{B}(\mathrm{X} \to \mathrm{VH})\,\mathcal{B}(\mathrm{H} \to \mathrm{b\bar{b}})$ in the combined heavy vector triplet hypothesis, for the combination of all the considered channels. The red and purple solid curves correspond to the cross sections predicted by the HVT model B ($g_\mathrm{V} = 3$) and model A ($g_\mathrm{V} = 1$), respectively.

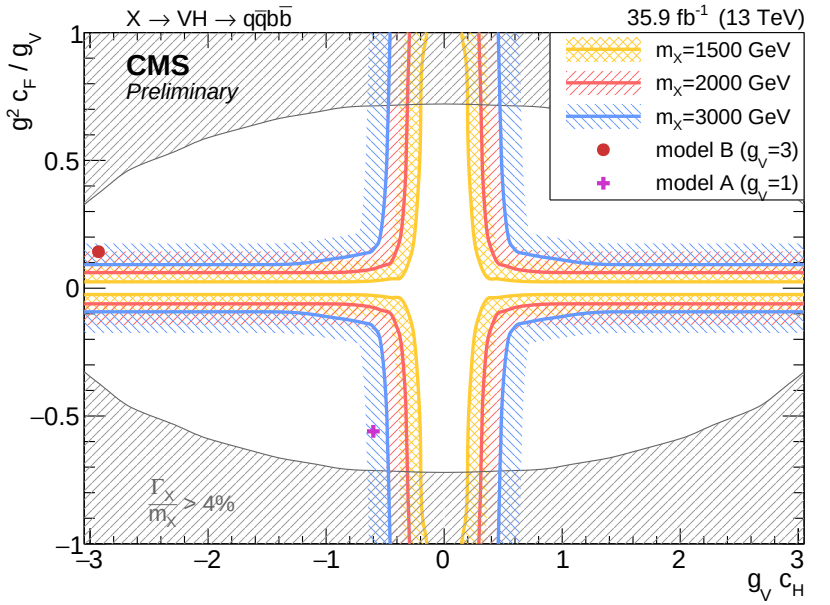

Figure 7: Observed exclusion in the HVT parameter plane $\left[g_\mathrm{V} c_\mathrm{H},\ g^2 c_\mathrm{F}/g_\mathrm{V}\right]$ for three different resonance masses (1.5, 2.0, and 3.0 TeV). The parameter g_V represents the coupling strength of the new interaction, c_H the coupling between the HVT bosons and the Higgs boson and longitudinally polarized SM vector bosons, and c_F the coupling between the heavy vector bosons and the SM fermions. The benchmark scenario corresponding to HVT model A ($g_\mathrm{V} = 1$) and model B ($g_\mathrm{V} = 3$) are represented by a purple cross and a red point. The gray shaded area corresponds to the region where the resonance natural width is predicted to be larger than the typical experimental resolution (4%), and thus the narrow-width approximation is not fulfilled.

9 Summary

A search for a heavy resonance with mass above 1 TeV and decaying into a vector boson and a Higgs boson, has been presented. The final states explored include the hadronic decay modes of the vector boson, and the decay of the Higgs boson to a $b\bar{b}$ pair. The data sample was collected by the CMS experiment at $\sqrt{s} = 13$ TeV during 2016, and corresponds to an integrated luminosity of 3.4 TeV. Depending on the resonance mass, upper limits in the range $0.8 - 50$ fb are set on the product of the cross section for a triplet of narrow spin-1 resonance and the branching fractions for the decay of the resonance into a Higgs and a vector boson, and for the decay of the Higgs boson into a pair of b quarks. The excluded resonance mass range is extended from 2.0 TeV to up to 3.4 TeV within the heavy vector triplet model in the benchmark scenario B ($g_V = 3$) with respect to the previous CMS searches, resulting in a significant reduction in the allowed parameter space for the large number of models generalized within the heavy vector triplet framework.

References

[1] ATLAS Collaboration, "Observation of a new particle in the search for the Standard Model Higgs boson with the ATLAS detector at the LHC", *Phys. Lett. B* **716** (2012) 1, doi:10.1016/j.physletb.2012.08.020, arXiv:1207.7214.

[2] CMS Collaboration, "Observation of a new boson at a mass of 125 GeV with the CMS experiment at the LHC", *Phys. Lett. B* **716** (2012) 30, doi:10.1016/j.physletb.2012.08.021, arXiv:1207.7235.

[3] CMS Collaboration, "Observation of a new boson with mass near 125 GeV in pp collisions at $\sqrt{s}$ = 7 and 8 TeV", *JHEP* **06** (2013) 081, doi:10.1007/JHEP06(2013)081, arXiv:1303.4571.

[4] ATLAS Collaboration, "Measurement of the Higgs boson mass from the $H \to \gamma\gamma$ and $H \to ZZ^* \to 4\ell$ channels in pp collisions at center-of-mass energies of 7 and 8 TeV with the ATLAS detector", *Phys. Rev. D* **90** (2014) 052004, doi:10.1103/PhysRevD.90.052004, arXiv:1406.3827.

[5] CMS Collaboration, "Precise determination of the mass of the Higgs boson and tests of compatibility of its couplings with the standard model predictions using proton collisions at 7 and 8 TeV", *Eur. Phys. J. C* **75** (2015) 212, doi:10.1140/epjc/s10052-015-3351-7, arXiv:1412.8662.

[6] CMS Collaboration, "Evidence for the direct decay of the 125 GeV Higgs boson to fermions", *Nat. Phys.* **10** (2014) 557, doi:10.1038/nphys3005, arXiv:1401.6527.

[7] ATLAS and CMS Collaborations, "Combined Measurement of the Higgs Boson Mass in pp Collisions at $\sqrt{s} = 7$ and 8 TeV with the ATLAS and CMS Experiments", *Phys. Rev. Lett.* **114** (2015) 191803, doi:10.1103/PhysRevLett.114.191803, arXiv:1503.07589.

[8] V. D. Barger, W.-Y. Keung, and E. Ma, "A gauge model with light W and Z bosons", *Phys. Rev. D* **22** (1980) 727, doi:10.1103/PhysRevD.22.727.

[9] E. Salvioni, G. Villadoro, and F. Zwirner, "Minimal Z' models: present bounds and early LHC reach", *JHEP* **09** (2009) 068, doi:10.1088/1126-6708/2009/11/068, arXiv:0909.1320.

[10] C. Grojean, E. Salvioni, and R. Torre, "A weakly constrained W′ at the early LHC", *JHEP* **07** (2011) 002, doi:10.1007/JHEP07(2011)002, arXiv:1103.2761.

[11] R. Contino, D. Pappadopulo, D. Marzocca, and R. Rattazzi, "On the effect of resonances in composite Higgs phenomenology", *JHEP* **10** (2011) 081, doi:10.1007/JHEP10(2011)081, arXiv:1109.1570.

[12] D. Marzocca, M. Serone, and J. Shu, "General composite Higgs models", *JHEP* **08** (2012) 13, doi:10.1007/JHEP08(2012)013, arXiv:1205.0770.

[13] B. Bellazzini, C. Csaki, and J. Serra, "Composite Higgses", *Eur. Phys. J. C* **74** (2014) 2766, doi:10.1140/epjc/s10052-014-2766-x, arXiv:1401.2457.

[14] T. Han, H. E. Logan, B. McElrath, and L.-T. Wang, "Phenomenology of the little Higgs model", *Phys. Rev. D* **67** (2003) 095004, doi:10.1103/PhysRevD.67.095004, arXiv:hep-ph/0301040.

[15] M. Schmaltz and D. Tucker-Smith, "Little Higgs Theories", *Ann. Rev. Nucl. Part. Sci.* **55** (2005) 229, doi:10.1146/annurev.nucl.55.090704.151502.

[16] M. Perelstein, "Little Higgs models and their phenomenology", *Prog. Part. Nucl. Phys.* **58** (2007) 247, doi:10.1016/j.ppnp.2006.04.001, arXiv:hep-ph/0512128.

[17] D. Pappadopulo, A. Thamm, R. Torre, and A. Wulzer, "Heavy vector triplets: bridging theory and data", *JHEP* **09** (2014) 60, doi:10.1007/JHEP09(2014)060, arXiv:1402.4431.

[18] CMS Collaboration, "Search for a pseudoscalar boson decaying into a Z boson and the 125 GeV Higgs boson in $\ell^+\ell^- b\bar{b}$ final states", *Phys. Lett. B* **748** (2015) 221, doi:10.1016/j.physletb.2015.07.010, arXiv:1504.04710.

[19] CMS Collaboration, "Search for a massive resonance decaying into a Higgs boson and a W or Z boson in hadronic final states in proton-proton collisions at $\sqrt{s} = 8$ TeV", *JHEP* **02** (2016) 145, doi:10.1007/JHEP02(2016)145, arXiv:1506.01443.

[20] CMS Collaboration, "Search for Narrow High-Mass Resonances in Proton-Proton Collisions at $\sqrt{s}$ = 8 TeV Decaying to a Z and a Higgs Boson", *Phys. Lett. B* **748** (2015) 255, doi:10.1016/j.physletb.2015.07.011, arXiv:1502.04994.

[21] CMS Collaboration, "Search for massive resonances decaying into WW, WZ, ZZ, qW and qZ in the dijet final state at $\sqrt{s} = 13$ TeV", CMS Physics Analysis Summary CMS-PAS-B2G-17-001, CERN, Geneva, 2017.

[22] CMS Collaboration, "Combination of diboson resonance searches at 8 and 13 TeV", CMS Physics Analysis Summary CMS-PAS-B2G-16-007, CERN, Geneva, 2016.

[23] CMS Collaboration, "Search for new resonances decaying to WW/WZ $\to \ell\nu$qq", CMS Physics Analysis Summary CMS-PAS-B2G-16-020, CERN, Geneva, 2016.

[24] CMS Collaboration, "Search for heavy resonances decaying into a Z boson and a W boson in the $\ell^+\ell^-$q$\bar{\text{q}}$ final state", CMS Physics Analysis Summary CMS-PAS-B2G-16-022, CERN, Geneva, 2017.

[25] ATLAS Collaboration, "Search for resonances with boson-tagged jets in 15.5 fb^{-1} of pp collisions at $\sqrt{s} = 13$ TeV collected with the ATLAS detector", CMS Physics Analysis Summary ATLAS-CONF-2016-055, CERN, Geneva, Aug, 2016.

[26] ATLAS Collaboration, "Search for diboson resonance production in the $\ell\nu qq$ final state using pp collisions at $\sqrt{s} = 13$ TeV with the ATLAS detector at the LHC", CMS Physics Analysis Summary ATLAS-CONF-2016-062, CERN, Geneva, Aug, 2016.

[27] ATLAS Collaboration, "Searches for heavy ZZ and ZW resonances in the llqq and vvqq final states in pp collisions at sqrt(s) = 13 TeV with the ATLAS detector", CMS Physics Analysis Summary ATLAS-CONF-2016-082, CERN, Geneva, Aug, 2016.

[28] CMS Collaboration, "Search for heavy resonances decaying into a vector boson and a Higgs boson in final states with charged leptons, neutrinos, and b quarks", *Phys. Lett. B* **768** (2017) doi:10.1016/j.physletb.2017.02.040, arXiv:1610.08066.

[29] ATLAS Collaboration, "Search for new resonances decaying to a W or Z boson and a Higgs boson in the $\ell^+\ell^- b\bar{b}$, $\ell\nu b\bar{b}$, and $\nu\bar{\nu}b\bar{b}$ channels with pp collisions at $\sqrt{s} = 13$ TeV with the ATLAS detector", *Phys. Lett. B* **765** (2016) doi:10.1016/j.physletb.2016.11.045, arXiv:1607.05621.

[30] ATLAS Collaboration, "A Search for Resonances Decaying to a W or Z Boson and a Higgs Boson in the $q\bar{q}^{(\prime)}b\bar{b}$ Final State", ATLAS Conference Note ATLAS-CONF-2016-083, CERN, Geneva, 2016.

[31] J. Alwall et al., "The automated computation of tree-level and next-to-leading order differential cross sections, and their matching to parton shower simulations", *JHEP* **07** (2014) 079, doi:10.1007/JHEP07(2014)079, arXiv:1405.0301.

[32] P. Nason, "A new method for combining NLO QCD with shower Monte Carlo algorithms", *JHEP* **11** (2004) 040, doi:10.1088/1126-6708/2004/11/040, arXiv:hep-ph/0409146.

[33] S. Frixione, P. Nason, and C. Oleari, "Matching NLO QCD computations with Parton Shower simulations: the POWHEG method", *JHEP* **11** (2007) 070, doi:10.1088/1126-6708/2007/11/070, arXiv:0709.2092.

[34] S. Alioli, P. Nason, C. Oleari, and E. Re, "A general framework for implementing NLO calculations in shower Monte Carlo programs: the POWHEG BOX", *JHEP* **06** (2010) 043, doi:10.1007/JHEP06(2010)043, arXiv:1002.2581.

[35] M. Czakon and A. Mitov, "Top++: A program for the calculation of the top-pair cross-section at hadron colliders", *Comput. Phys. Commun.* **185** (2014) 2930, doi:10.1016/j.cpc.2014.06.021, arXiv:1112.5675.

[36] T. Sjöstrand, S. Mrenna, and P. Skands, "A brief introduction to PYTHIA 8.1", *Comput. Phys. Commun.* **178** (2008) 852, doi:10.1016/j.cpc.2008.01.036, arXiv:0710.3820.

[37] T. Sjöstrand, S. Mrenna, and P. Skands, "PYTHIA 6.4 physics and manual", *JHEP* **05** (2006) 026, doi:10.1088/1126-6708/2006/05/026, arXiv:hep-ph/0603175.

[38] P. Skands, S. Carrazza, and J. Rojo, "Tuning PYTHIA 8.1: the Monash 2013 Tune", *Eur. Phys. J. C* **74** (2014) 3024, doi:10.1140/epjc/s10052-014-3024-y, arXiv:1404.5630.

[39] CMS Collaboration, "Event generator tunes obtained from underlying event and multiparton scattering measurements", *Eur. Phys. J. C* **76** (2016) 155, doi:10.1140/epjc/s10052-016-3988-x, arXiv:1512.00815.

[40] CMS Collaboration, "Investigations of the impact of the parton shower tuning in Pythia 8 in the modelling of $\mathrm{t\bar{t}}$ at $\sqrt{s} = 8$ and 13 TeV", CMS Physics Analysis Summary CMS-PAS-TOP-16-021, CERN, Geneva, 2016.

[41] NNPDF Collaboration, "Parton distributions for the LHC Run II", *JHEP* **04** (2015) 040, doi:10.1007/JHEP04(2015)040, arXiv:1410.8849.

[42] GEANT4 Collaboration, "GEANT4—a simulation toolkit", *Nucl. Instrum. Meth. A* **506** (2003) 250, doi:10.1016/S0168-9002(03)01368-8.

[43] CMS Collaboration, "Description and performance of track and primary-vertex reconstruction with the CMS tracker", *JINST* **9** (2014) P10009, doi:10.1088/1748-0221/9/10/P10009, arXiv:1405.6569.

[44] CMS Collaboration, "The CMS experiment at the CERN LHC", *JINST* **3** (2008) S08004, doi:10.1088/1748-0221/3/08/S08004.

[45] CMS Collaboration, "The CMS trigger system", *JINST* **12** (2017) P01020, doi:10.1088/1748-0221/12/01/P01020, arXiv:1609.02366.

[46] CMS Collaboration, "Particle-flow event reconstruction in CMS and performance for jets, taus, and $E_{\mathrm{T}}^{\mathrm{miss}}$", CMS Physics Analysis Summary CMS-PAS-PFT-09-001, CERN, 2009.

[47] CMS Collaboration, "Commissioning of the particle-flow event with the first LHC collisions recorded in the CMS detector", CMS Physics Analysis Summary CMS-PAS-PFT-10-001, CERN, 2010.

[48] M. Cacciari, G. P. Salam, and G. Soyez, "The anti-k_{t} jet clustering algorithm", *JHEP* **04** (2008) 063, doi:10.1088/1126-6708/2008/04/063, arXiv:0802.1189.

[49] CMS Collaboration, "Pileup Removal Algorithms", CMS Physics Analysis Summary CMS-PAS-JME-14-001, CERN, Geneva, 2014.

[50] M. Cacciari, G. P. Salam, and G. Soyez, "FastJet user manual", *Eur. Phys. J. C* **72** (2012) 1896, doi:10.1140/epjc/s10052-012-1896-2, arXiv:1111.6097.

[51] M. Cacciari, G. P. Salam, and G. Soyez, "The catchment area of jets", *JHEP* **04** (2008) 005, doi:10.1088/1126-6708/2008/04/005, arXiv:0802.1188.

[52] CMS Collaboration, "Jet energy scale and resolution in the CMS experiment in pp collisions at 8 TeV", *JINST* **12** (2017), no. 02, P02014, doi:10.1088/1748-0221/12/02/P02014, arXiv:1607.03663.

[53] D. Bertolini, P. Harris, M. Low, and N. Tran, "Pileup per particle identification", *Journal of High Energy Physics* **2014** (2014) 59, doi:10.1007/JHEP10(2014)059.

[54] M. Dasgupta, A. Fregoso, S. Marzani, and G. P. Salam, "Towards an understanding of jet substructure", *JHEP* **09** (2013) 029, doi:10.1007/JHEP09(2013)029, arXiv:1307.0007.

[55] A. J. Larkoski, S. Marzani, G. Soyez, and J. Thaler, "Soft drop", *JHEP* **05** (2014) 146, doi:10.1007/JHEP05(2014)146, arXiv:1402.2657.

[56] CMS Collaboration, "Identification techniques for highly boosted W bosons that decay into hadrons", *JHEP* **12** (2014) 017, doi:10.1007/JHEP12(2014)017, arXiv:1410.4227.

[57] J. Thaler and K. Van Tilburg, "Identifying Boosted Objects with N-subjettiness", *JHEP* **03** (2011) 015, doi:10.1007/JHEP03(2011)015, arXiv:1011.2268.

[58] CMS Collaboration, "Identification of double-b quark jets in boosted event topologies", CMS Physics Analysis Summary CMS-PAS-BTV-15-002, CERN, Geneva, 2016.

[59] D. Krohn, J. Thaler, and L.-T. Wang, "Jet Trimming", *JHEP* **02** (2010) 084, doi:10.1007/JHEP02(2010)084, arXiv:0912.1342.

[60] M. Bähr et al., "Herwig++ physics and manual", *Eur. Phys. J. C* **58** (2008) 639, doi:10.1140/epjc/s10052-008-0798-9, arXiv:0803.0883.

[61] CMS Collaboration, "CMS Luminosity Measurement for the 2016 Data Taking Period", CMS Physics Analysis Summary CMS-PAS-LUM-17-001, CERN, 2017.

[62] J. Butterworth et al., "PDF4LHC recommendations for LHC Run II", *J. Phys. G* **43** (2016) 23001, doi:10.1088/0954-3899/43/2/023001, arXiv:1510.03865.

[63] T. Junk, "Confidence level computation for combining searches with small statistics", *Nucl. Instrum. Meth. A* **434** (1999) 435, doi:10.1016/S0168-9002(99)00498-2, arXiv:hep-ex/9902006.

[64] A. L. Read, "Presentation of search results: the CL_s technique", *J. Phys. G* **28** (2002) 2693, doi:10.1088/0954-3899/28/10/313.

[65] CMS and ATLAS Collaborations, "Procedure for the LHC Higgs boson search combination in Summer 2011", CMS Note CMS-NOTE-2011-005, ATL-PHYS-PUB-2011-11, CERN, 2011.

[66] G. Cowan, K. Cranmer, E. Gross, and O. Vitells, "Asymptotic formulae for likelihood-based tests of new physics", *Eur. Phys. J. C* **71** (2011) 1554, doi:10.1140/epjc/s10052-011-1554-0, arXiv:1007.1727. [Erratum: doi:10.1140/epjc/s10052-013-2501-z].